

Abstract

Surface-based radon (^{222}Rn) measurements can be combined with lidar backscatter to obtain a higher quality time series of mixing height within the Planetary Boundary-Layer (PBL) than is possible from lidar alone, and a more quantitative measure of mixing height than is possible from only radon. The lidar measurements benefit because even when aerosol layers are detected, reliably attributing the mixing height to the correct layer presents a challenge. By combining lidar with a mixing length scale derived from a time series of radon concentration, automated and robust attribution is possible during the morning transition.

Radon measurements also provide mixing information during the night and with the addition of lidar these measurements become insensitive to night-to-night changes in radon emissions. After calibration with lidar, the radon-derived equivalent mixing height agrees with other measures of mixing on daily and hourly time scales and is a potential method for studying intermittent mixing in nocturnal boundary layers.

1 Introduction

The state of the planetary boundary layer is one of the factors controlling surface-atmosphere interactions. In particular, changes in surface forcing lead to changes in boundary layer state on time scales of less than one hour, and vice-versa (Stull, 1988). The boundary layer mixing height, h , is a key parameter describing its state and is central to predicting the fate of pollutants and trace gases emitted at the surface (Arya, 1999), as well being important for the development and testing of boundary layer parametrisation schemes in weather and climate models (Vogelezang and Holtlag, 1996).

A number of techniques employing surface-based instruments are currently used for continuous observations of the mixing height (Emeis et al., 2008), one of which uses elastic backscatter lidar. This approach relies upon the detection of laser light that is

Improved mixing height monitoring

A. D. Griffiths et al.

Title Page

Abstract

Introduction

Conclusions

References

Tables

Figures

◀

▶

◀

▶

Back

Close

Full Screen / Esc

Printer-friendly Version

Interactive Discussion



Improved mixing height monitoring

A. D. Griffiths et al.

Title Page	
Abstract	Introduction
Conclusions	References
Tables	Figures
◀	▶
◀	▶
Back	Close
Full Screen / Esc	
Printer-friendly Version	
Interactive Discussion	



scattered back to a detector by molecules and aerosols in the air column. Assuming a large drop in aerosol abundance across the interface between the mixing layer and the overlying free atmosphere, mixing height can then be tracked over time by processing the range-resolved backscatter signal (Lammert and Bösenberg, 2006; Emeis et al., 2008; Baars et al., 2008). Although this approach works well under favourable conditions, the development of a mixing height algorithm that is both automated and widely applicable remains a significant challenge. This is all the more important as new low-power lidars designed for detecting cloud base (i.e. ceilometers) can also be used for determining mixing height (Münkel, 2007; Emeis et al., 2009, 2012). While ceilometers have lower signal-to-noise ratios than lidars, they are less expensive to purchase and maintain and are becoming deployed more widely in growing networks (Haeffelin et al., 2012).

Lidar-based mixing height determination is essentially a two step process: detection and attribution. In the detection step, the tops of distinct atmospheric layers are identified; the attribution step involves assigning the height of one of the detected layers to the current mixing height. Of these steps, attribution poses the larger challenge (Haeffelin et al., 2012). Indeed the information available from an elastic-scattering lidar may be insufficient for successful attribution, so some schemes incorporate supplementary information, either from model output (Di Giuseppe et al., 2012) or additional sensors (Emeis et al., 2004).

At certain times, even the detection stage fails. For instance, many lidars are blind to backscatter from the closest tens to hundreds of meters and are therefore unable to detect shallow mixing heights typical of inland nocturnal boundary layers. It is possible to overcome this problem by using common optics for both the transmitter and receiver, i.e. a monostatic design like some ceilometers, or by photographing the beam side-on with a wide-angle digital camera (Barnes et al., 2007; Sharma et al., 2011). Even then the presence of multiple aerosol layers, or absence of a strong contrast at the top of the mixed layer, may preclude mixing height detection using lidar. In such cases, an alternative method entirely needs to be sought.

Improved mixing height monitoring

A. D. Griffiths et al.

Title Page

Abstract

Introduction

Conclusions

References

Tables

Figures

◀

▶

◀

▶

Back

Close

Full Screen / Esc

Printer-friendly Version

Interactive Discussion



Monitoring diurnal changes in the concentration of well constrained passive tracers provides an alternative to lidar for quantifying vertical mixing near the surface. Radon-222 is a naturally occurring passive tracer, chemically inert and released from the surface at a relatively constant rate. Atmospheric profiles of radon measured from aircraft (Williams et al., 2011), or gradient measurement from towers (Chambers et al., 2011; Grossi et al., 2012; Moses et al., 1960), can be used to study mixing processes. Due to the simplicity of processes affecting radon concentration, with a few assumptions it is possible to derive an “equivalent mixing height” from a time series of near surface radon concentrations for part of the diurnal cycle.

The equivalent mixing height, h_e , is defined from the accumulation of near-surface radon at night and then dilution the following morning (Allegrini et al., 1994; Fontan et al., 1979; Guedalia et al., 1980; Pasini and Ameli, 2003; Sesana et al., 2003, 2006; Keller et al., 2011). At inland sites h_e is closely linked to the actual mixing height, and corresponds exactly when the boundary layer is well mixed, an assumption for the derivation of h_e . This measure of mixing, however, can not be applied equally to the whole diurnal cycle; its suitability is restricted to the period between late afternoon, when a stable boundary layer first begins to form, and mid-morning, some time before the transition from the nocturnal stable boundary layer to a fully-developed convective boundary layer is complete.

When used in isolation the radon-based mixing height estimate is unconstrained because of the uncertainty in surface radon emissions. Fontan et al. (1979) used tower measurements to estimate emissions, but also pointed out that remote sensing (specifically, sodar) would be a viable alternative.

Under typical fair-weather conditions, at a rural inland site, neither lidar nor radon measurements can be used to determine the mixing height over the full diurnal cycle. In the mid afternoon, when the boundary layer is fully developed and actively mixing, lidar, but not radon, can be used to determine the mixing height. The onset of stable stratification near the surface, which comes with the changing radiation balance in the late afternoon, is undetectable to lidar, but is clearly marked by an increasing surface

355 nm including both molecular and aerosol scattering; α is the extinction coefficient at 355 nm; and B is the combined electronic and optical background.

The range-corrected backscatter signal, $S(r)$, is the range-resolved power corrected for background, overlap and range:

$$S(r) = [P(r) - B]r^2/\xi(r). \quad (2)$$

Range-corrected backscatter is expressed in arbitrary units. Lidar results are expressed this way because, in well-mixed regions where β and α are constants, a plot of r versus $\log S$ is a straight line.

During this deployment, the 10 min lidar measurement cycle includes five minutes of operation followed by a five minute pause. Throughout the experiment the beam was angled at 30° above the western horizon, thus halving the minimum measurement height compared with a vertically aligned beam, and doubling the vertical resolution, to 7.5 m. Furthermore, compared with a vertically aligned beam, the signal-to-noise ratio at a given height is reduced by a factor of about $2^{3/2} \approx 2.8$, neglecting absorption.

Mixing heights were derived following a procedure based on the "STRAT-2D" method (Haeffelin et al., 2012). For each five minute block, S was averaged, and then the results arranged in a two dimensional array as a function of time and range. To further increase the signal to noise ratio, a Gaussian filter was then applied with a width at half-maximum of one point in the time direction and three points in the height direction. The magnitude of the two-dimensional gradient was then computed over the smoothed S array.

At each time step, heights where the 2-D gradient reached a local minimum were identified and three candidates for the mixing height were chosen from these. These were: (1) where the magnitude of the gradient was largest, (2) second-largest, and (3) the closest local maximum to the surface.

Two example lidar profiles, one with a detectable mixing height, and one without, are shown in Fig. 2.

Improved mixing height monitoring

A. D. Griffiths et al.

Title Page

Abstract

Introduction

Conclusions

References

Tables

Figures

◀

▶

◀

▶

Back

Close

Full Screen / Esc

Printer-friendly Version

Interactive Discussion



2.3 The radon-based equivalent mixing height

Since near-surface radon concentrations are strongly affected by vertical mixing, in principle a mixing length scale can be computed from a time series of radon concentration. But once the boundary layer is fully developed in the afternoon, advection becomes comparably more important, so we focus only on the period between the establishment of stable stratification in the late afternoon until a few hours into the morning transition. Furthermore, while computing this length scale we assume that radon emissions are constant each night, although they may change night-to-night.

To compute a mixing length from radon concentrations we use a boundary layer box-model. This is a minor elaboration of one proposed by Sesana et al. (2003) which itself is based on an earlier model (Fontan et al., 1979). Radon emissions, F , are horizontally homogeneous and constant in time; the flow-field is non-divergent; horizontal advection of radon is neglected; and surface emissions are instantaneously mixed to a height h_e , so that radon concentrations, C , in this layer are constant with height. At $z = h_e$ there is a step change in radon concentration from C to C_r , the residual concentration from a previous, deeper, mixed layer. Multiple residual layers are permitted above h_e , and these are impacted only by radioactive decay.

Under these conditions, the change in radon concentration within the lower well-mixed layer is due to a balance between surface emissions, radioactive decay and, if the layer is growing, dilution. Writing these terms in order we have

$$\frac{dC}{dt} = F/h_e - \lambda C - D \quad (3)$$

where $\lambda = 2.09822 \times 10^{-6} \text{ s}^{-1}$ is the radon-222 decay constant and D is the dilution term, $D = 0$ if $dh_e/dt \leq 0$ and

$$D = \frac{C - C_r}{h_e} \frac{dh_e}{dt} \quad (4)$$

if h_e is growing with time.

Improved mixing height monitoring

A. D. Griffiths et al.

Title Page

Abstract

Introduction

Conclusions

References

Tables

Figures

◀

▶

◀

▶

Back

Close

Full Screen / Esc

Printer-friendly Version

Interactive Discussion



Improved mixing height monitoring

A. D. Griffiths et al.

Title Page

Abstract

Introduction

Conclusions

References

Tables

Figures

◀

▶

◀

▶

Back

Close

Full Screen / Esc

Printer-friendly Version

Interactive Discussion



The initial concentration each day is set to the afternoon minimum near-surface radon concentration. The boundary layer is assumed to be well mixed at this time because vertical gradients are negligible compared with the nocturnal peak, e.g. 0.2 Bq m^{-3} between 2 and 50 m (Moses et al., 1960; Chambers et al., 2011). The first estimate of surface emissions ($30 \text{ mBq m}^{-2} \text{ s}^{-1}$) is taken from Griffiths et al. (2010), although we refine these in Sect. 2.4.

To compute h_e we start by identifying the establishment of a stable boundary layer in the afternoon and then iterate forwards using a finite-difference approximation to Eqs. (3) and (4), as detailed in Appendix A.

An alternative method of deriving h_e (Fontan et al., 1979), is to set $D = 0$ and use the analytical solution of Eq. (3) to obtain

$$h_{\text{acc}} = \frac{F(1 - e^{-\lambda t})}{\lambda(C - e^{-\lambda t}C_0)} \quad (5)$$

where we here call h_{acc} the accumulated equivalent mixing height. In Eq. (5), C_0 is the concentration at time $t = 0$, the time when radon concentration reaches its minimum.

Example output from each of the methods is shown in Fig. 3, indicating that h_{acc} and h_e are equal only when mixing is deeper than earlier in the night; for periods of shallower mixing $h_{\text{acc}} > h_e$. Based on this example, h_{acc} is more sensitive to the history of mixing, remaining elevated after a burst of mixing, whereas h_e returns to its earlier value.

To estimate the uncertainty in h_e we generate a 1000-member ensemble of radon concentration time series and compute h_e time series from each. For each ensemble member, the radon concentration at each time step is the observed radon concentration plus a random perturbation drawn from a distribution with the same standard deviation as the measurement uncertainty reported by the AlphaGuard. The uncertainty in h_e is then computed from the ensemble spread at each time step.

2.4 Combining radon with lidar

As shown in Sect. 2.3, equivalent mixing height depends on the surface radon emissions, F . Although long-term mean emissions are relatively well characterised on large scales (Conen and Robertson, 2002; Griffiths et al., 2010; Szegvary et al., 2009; Zhang et al., 2011) there are also night-to-night fluctuations (which sometimes change emissions by a factor of two; Holford et al., 1993; Schery et al., 1984) and local variability, which makes F dependent on the changing measurement footprint. The dependence on measurement footprint, at this site in particular with large and spatially-variable radon emissions (Fig. 1), compromises the suitability of spot accumulation chamber measurements to characterise radon emissions, so an alternative method is required.

To constrain the nightly radon emissions, we use the period where both the lidar and radon-based measurements are applicable. As discussed in Sect. 1, this period begins in the morning when the mixing height grows large enough to be observed with lidar and ends when the error in h_e becomes large, around midday.

In order to merge the lidar and radon measurements we define and minimize a cost function, R while varying the equivalent mixing height by scaling it by an arbitrary factor, s . This selection process is performed independently for each morning, thereby accounting for possible night-to-night changes in radon emissions.

To perform the merge, we first interpolate the hourly h_e time series during the morning transition to match the 10 min lidar averaging period. For a set of interpolated points $\{h_{e0}, h_{e1}, \dots, h_{eN}\}$, and a particular guess of the scale factor, s , the cost function is defined as

$$R(s) = \sum_{i=0}^N \min_j (sh_{ei} - \tilde{h}_{ij})^2 w_{ij} \quad (6)$$

where \tilde{h}_{ij} represents the j th candidate mixing heights (there are three at each time step) from the lidar at the i th time step.

Improved mixing height monitoring

A. D. Griffiths et al.

Title Page

Abstract

Introduction

Conclusions

References

Tables

Figures

◀

▶

◀

▶

Back

Close

Full Screen / Esc

Printer-friendly Version

Interactive Discussion



Improved mixing height monitoring

A. D. Griffiths et al.

Title Page

Abstract

Introduction

Conclusions

References

Tables

Figures

◀

▶

◀

▶

Back

Close

Full Screen / Esc

Printer-friendly Version

Interactive Discussion



The weights, $w_{ij} = (\sigma_{h_e}^2 + \sigma_{\tilde{h}_{ij}}^2)^{-1}$, reflect the combined uncertainty of h_e and h . The uncertainty in h_e at the 10 minute scale, σ_{h_e} , is interpolated from the point-by-point estimate in the uncertainty in h_e at the hourly scale. The uncertainty in h_e may be asymmetric around the mean value of h_e , since it is computed from ensemble statistics, as described in Appendix A. Initially $\sigma_{\tilde{h}_{ij}}$ was based on the height resolution of the lidar (7.5 m), thereby neglecting other sources of error. It was then tuned for the best performance of the merging algorithm and set to a constant value of 15 m. This is not intended as a rigorous estimate of measurement uncertainty, however, nor is it required to be.

After minimising the cost function (using a global search), mixing heights and the radon flux for that night are obtained. The radon emissions are

$$F = F_0 s_{\min} \quad (7)$$

where F_0 is the original guess of the radon flux. Likewise, h_e is calibrated for nightly variations by it scaling by the same factor, s_{\min} . In addition the set of \tilde{h}_{ij} points which minimise $R(s)$ are retained as the “best-estimate” mixing height during the period with overlapping lidar and radon data.

3 Results and discussion

Conditions throughout the two-week observation period were predominantly clear with few clouds below 5 km. The main exceptions were the period 2–3 May, characterised by precipitating cumulus or stratus cloud with a base around 2 km a.g.l., and several days when non-precipitating boundary layer cumulus developed after midday.

The observed hourly radon concentrations (Fig. 4a) exhibit a large diurnal range, typical of an inland site under clear skies. The amplitude of the nocturnal peaks is related to the degree of atmospheric stability and the strength of local radon emissions, whereas variations in the daytime minimum radon concentration, about 1–8 Bq m⁻³ are

Improved mixing height monitoring

A. D. Griffiths et al.

Title Page

Abstract

Introduction

Conclusions

References

Tables

Figures

◀

▶

◀

▶

Back

Close

Full Screen / Esc

Printer-friendly Version

Interactive Discussion



dominated by long-range fetch and the maximum daytime mixing height (Chambers et al., 2011). The large nocturnal peaks, relative to the daytime minima, suggest that vertical mixing is the main process affecting the diurnal cycle in this dataset. As a result, this is a promising time series from which to compute an equivalent mixing height. The calculated equivalent mixing heights (Fig. 4b), exhibit a variability that follows naturally from the radon time series: the smallest equivalent mixing heights are associated with the highest nocturnal radon concentrations.

As well as the large night-to-night variability evident in equivalent mixing height (averages for each night range from 10 to 125 m with a median of 45 m) considerable variability is also seen within each night. While this is sometimes a result of measurement uncertainty there are also variations in equivalent mixing height well outside the range of measurement uncertainty, which is indicated by the shading in Fig. 4b. After sunrise each day the surface radon concentration falls and h_e grows, as does the uncertainty in h_e . Around midday, when $h_e \gtrsim 1$ km, h_e estimates become unreliable.

Figure 4c summarises the results of merging the radon- and lidar-based mixing heights following the method described in Sect. 2.4. Average radon emissions calculated by this technique were $56 \text{ mBq m}^2 \text{ s}^{-1}$ for the entire measurement period. This is higher than the expected value of around $30 \text{ mBq m}^2 \text{ s}^{-1}$ but within the estimated range of emissions near the site (Sect. 2.1). Nightly estimates of radon emissions ranged between 40 and $80 \text{ mBq m}^2 \text{ s}^{-1}$, possibly due to the significant horizontal gradients in radon emissions nearby (Fig. 1) combined with variations in the strength of drainage flows which are not taken into account. Such flows are common at night in rolling terrain (Soler et al., 2002) and may lead to radon accumulation at the measurement site, which is near the bottom of a low hill, thereby increasing the effective flux.

3.1 Using radon to improve lidar

The automatic procedure for combining the two data types worked well, with the exception of the mornings of 2 May, and 7 May. On 2 May, low clouds and precipitation led to a complicated boundary layer structure and no suitable mixing height candidates were

detected, while on 7 May the attribution step failed. Two aerosol layers were evident on 7 May and the radon mixing height was fit between the two. On two other days, the radon-derived mixing height led or lagged the lidar-derived mixing height by up to an hour, most likely attributable to the combination of rolling terrain and spatial separation (1.5 km) between the radon detector and lidar.

Figure 5 shows examples of the three potential merging outcomes (success, failure, or time lag) in more detail: on 6 May the fit was successful, on 7 May the fit failed due to ambiguities in the lidar data, and on 8 May there was a temporal lag between the lidar-derived and radon-derived mixing heights. As well as showing the final set of best-match points, this figure also includes the candidate points from the detection stage of the algorithm, most of which have been rejected after merging the lidar and h_e time series.

It may be possible, in future studies, to overcome the problems that have led here to unsuccessful or lagged matches. As formulated, the matching method necessitates merging of the two data streams during the morning transition, a period of rapidly changing mixing height. Under these conditions, collocating the lidar and radon detector might reduce, or remove, the observed lag between the two measurements. Furthermore, the seemingly incorrect attribution on 7 May could perhaps be rectified by using a more sophisticated merging algorithm, as might be achieved by applying the additional constraints described by Haeffelin et al. (2012). However, there will be days where the merging procedure fails or produces uncertain results. Examples are: when the mixing height grows rapidly through the range where merging is possible, so that the merging process hinges on a small number of data points; when synoptic systems bring air to the measurement site with higher or lower radon concentrations; or when radon fluxes change during the night, perhaps from a rainfall event.

For the merging procedure to work well for routine operations, there are improvements which should be made, probably by incorporating radon into an established lidar processing scheme. But leaving this aside, Figs. 4 and 5 clearly demonstrate that the

Improved mixing height monitoring

A. D. Griffiths et al.

Title Page

Abstract

Introduction

Conclusions

References

Tables

Figures

◀

▶

◀

▶

Back

Close

Full Screen / Esc

Printer-friendly Version

Interactive Discussion



radon-derived equivalent mixing height is indeed useful for constraining the attribution step in a lidar mixing height detection strategy.

3.2 Using lidar to improve radon measurements

In the preceding section, we have demonstrated that simultaneous radon measurements can improve the quality of mixing height derived from lidar measurements. However the converse is also true.

One of the products of merging radon and lidar-derived mixing heights is a night-by-night measure of radon emissions, F , which can be used to estimate fluxes of other trace gases. This can be combined with the radon concentration measurements, C , and an additional measurement of a surface-emitted tracer, ϕ , with unknown surface emissions F_ϕ . The unknown surface emissions can be estimated from (Conen et al., 2002)

$$\frac{\Delta\phi}{\Delta C} = \frac{F_\phi}{F} \quad (8)$$

where $\Delta\phi$ and ΔC represent changes in ϕ and C over a common time period. This technique has been used to measure trace gas fluxes in grassland (Obrist et al., 2006) and forests (Martens et al., 2004; Trumbore et al., 1990; Ussler et al., 1994).

Beyond this, the interpretation of h_e itself bears further investigation. As the nocturnal boundary layer is rarely well mixed, h_e is not directly comparable to more usual definitions of the mixing height (Seibert et al., 2000; Vickers and Mahrt, 2004) and should instead be interpreted as an integral length scale for mixing. In addition, h_e depends on measurement height, due to the strong near-surface gradient in radon concentrations under stable conditions.

Furthermore, it remains to be established whether calibration with lidar makes any difference to how well h_e describes mixing height, or whether h_e , computed from hour-to-hour changes in radon concentration, can be demonstrated to be better than h_{acc} ,

Improved mixing height monitoring

A. D. Griffiths et al.

Title Page

Abstract

Introduction

Conclusions

References

Tables

Figures

◀

▶

◀

▶

Back

Close

Full Screen / Esc

Printer-friendly Version

Interactive Discussion



computed from accumulation since the start of the night, as an indicator of mixing height.

We investigate these issues below on whole-night and hourly time scales.

3.2.1 Nightly average h_e variations related to mixing

5 The depth of the nocturnal stable boundary layer is determined from a balance between radiative cooling of the surface, which acts to reduce mixing height, and mechanical wind-driven turbulence, which acts to increase mixing height. Higher wind speeds at the surface are usually an indication of deeper mixing, since wind speed is closely linked to turbulence intensity. Conversely, very shallow mixing is associated with the
10 decoupling of the surface from the geostrophic wind aloft, and therefore near-calm conditions in the absence of drainage flows (e.g. Mahrt, 1999).

Because our data comes from nights with predominantly clear skies (conductive to strong radiative cooling of the surface), we assume that higher wind speeds are associated with deeper mixing. Consequently, if night-time mean wind speed is correlated
15 with night-time mean equivalent mixing height, it is most likely that night-to-night variations in h_e are related to changes in the depth of mixing, and are not an artefact of the method.

In Fig. 6 the nightly average wind speed (from 1800–0600 lt) is compared with the corresponding nightly average equivalent mixing height, h_e . Without applying the lidar-derived calibration, the relationship between equivalent mixing height and wind speed
20 is consistent with the interpretation that night-to-night changes in h_e can be regarded as night-to-night changes in mixing. After calibration, also shown in Fig. 6, the linearity of this relationship is degraded (the coefficient of determination, r^2 , decreases from 0.80 to 0.69) since, on some nights, the fitting process produced suboptimal results
25 (Sect. 3.1).

Calibration is necessary to reduce the bias in mixing heights and it is desirable to take changes in radon emissions into account. For a longer observation period, however, it

Improved mixing height monitoring

A. D. Griffiths et al.

Title Page

Abstract

Introduction

Conclusions

References

Tables

Figures

◀

▶

◀

▶

Back

Close

Full Screen / Esc

Printer-friendly Version

Interactive Discussion



may be useful to assume that radon emissions remain constant for N nights, choosing N to minimise the scatter in a plot similar to Fig. 6.

3.2.2 Hourly variations in h_e related to mixing

The approach taken here of computing h_e according to hourly changes in radon concentration allows us to detect temporary increases in the mixing height during the night. This is desirable, since intermittent turbulence is a central feature of stable boundary layers (Banta et al., 2007; Mahrt, 1999; Sun et al., 2004), but means that h_e is more sensitive to measurement noise or concentration fluctuations caused by effects other than vertical mixing. An alternative method, less sensitive to such fluctuations, is to calculate h_e on an accumulated basis, i.e. h_{acc} which is computed from the total increase in radon concentration since the start of the night according to Eq. (5). However, our measurements are from an inland site, with a high signal-to-noise ratio, so it is conceivable that fluctuations in h_e are primarily the result of intermittent mixing.

To support this hypothesis we examine both a one-night case study and the relationship between h_e and the bulk Richardson number over a longer period. Figure 7 shows several time series covering a strongly stable night punctuated by a mixing burst, which is consistent with the mechanism for intermittent turbulence described by Van de Wiel et al. (2002). The bulk Richardson number (Ri_b ; Glickman, 2000) shows that the stability in the lowest 7.5 m of the air column increases after sunset and enters the strongly stable regime, $Ri_b > 1$ (Mahrt, 2010). A burst of mixing occurs shortly after midnight, revealed by an abrupt drop in the bulk Richardson number, but also visible as a sudden increase in wind speed and a cessation of net cooling at 2 m a.g.l.

The mixing burst is also apparent in the time series of equivalent mixing height. The growth in h_e is not as abrupt as the drop in Ri_b , but the timing is similar. After the return to very stable conditions, h_e returns to its pre-event value. Nevertheless, h_{acc} remains elevated because of its dependence on the radon concentration history. Because of the correspondence between fluctuations in h_e and Ri_b , there is little doubt that the h_e peak on this night, and similar peaks on other nights (shown in Fig. 4), are due to

Improved mixing height monitoring

A. D. Griffiths et al.

Title Page

Abstract

Introduction

Conclusions

References

Tables

Figures

◀

▶

◀

▶

Back

Close

Full Screen / Esc

Printer-friendly Version

Interactive Discussion



transient mixing. It is apparent that h_e is preferable to h_{acc} for studying these transient events.

Figure 8 shows lidar-calibrated h_e versus the bulk Richardson number, for a subset of the full 2-week period (due to instrumentation drop-outs). Large values of h_e are only observed only under unstable conditions when $Ri_b < 0$, but a wide range of Ri_b values are possible for small h_e . This is indicative both of a relationship between h_e and Ri_b and that the two quantities carry different information. For instance, it is possible to have an unstable, but shallow, mixing layer early in the morning before the mixing layer is fully developed. Although not shown here, plots of uncalibrated h_e versus Ri_b , or h_{acc} versus Ri_b , show a similar relationship. In agreement with the conclusions from the single night in Fig. 7, there is a clearer relationship, with a greater tendency for small equivalent mixing heights under stable conditions, for h_e than for h_{acc} .

When considering data at the hourly scale the equivalent mixing height presents as a useful measure of mixing, and is most useful when computed from hour-by-hour changes in radon concentration. Calibration with lidar reduces biases, but can increase scatter because of uncertainties in the merging process.

4 Conclusions

By combining radon and lidar measurements of boundary layer mixing we can benefit from the complimentary strengths of the two techniques. The radon-derived equivalent mixing height benefits from simultaneous lidar measurements which allow calibration for the effect of short term and fetch-related changes in radon emissions.

Radon measurements, meanwhile, improve the lidar retrievals of mixing height by helping to correctly identify the mixing height from a set of candidates during the morning transition. Radon measurements also clearly mark the establishment of a stable boundary layer in the evening, which is undetectable by lidar. In monetary terms, radon detectors are a fraction of the cost of commercial lidar systems and have a low maintenance requirement. Consequently, even a modest improvement in the reliability

Improved mixing height monitoring

A. D. Griffiths et al.

Title Page

Abstract

Introduction

Conclusions

References

Tables

Figures

◀

▶

◀

▶

Back

Close

Full Screen / Esc

Printer-friendly Version

Interactive Discussion



of mixing height retrievals might justify the expense of simultaneous radon observations.

There is potential for this technique to be widely used at other inland sites, particularly since we expect the approach to be equally suited for mixing height retrievals from
5 ceilometers.

Appendix A

Finite-difference implementation of the box model

The well-mixed box model, introduced in Sect. (2.3), is used to compute the equivalent mixing height, h_e , from hourly-average radon concentration measurements. Here we
10 describe the specifics of its implementation.

The state of the box model at time-step i is represented by a piecewise-constant radon profile, $C_p^{(i)}(z)$, and $h_e^{(i)}$ where z is distance above the surface. Radon is always well mixed between $z = 0$ and $h_e^{(i)}$ and equal to the observed radon concentration, $C^{(i)}$. Above $h_e^{(i)}$ no mixing occurs but residual radon persists from earlier deep mixing.

The model is initialized when observed radon concentrations begin increasing in the late afternoon due to the formation of a stable boundary layer, defined as time $t = 0$. Initially, $C_p^{(0)}$ is set to the daytime minimum radon concentration and $h_e^{(0)}$ is undefined.

To advance the model forward in time, a finite difference approximation to Eq. (3) is applied so that

$$\frac{C^{(i)} - C^{(i-1)}}{\Delta t} = \frac{F}{h_e^{(i)}} - \lambda C^{(i-1)} - D^{(i)} \quad (\text{A1})$$

where Δt is the time between observations, F is the radon surface flux, λ is the decay constant for radon-222, and D is dilution caused by the entrainment of air during periods of mixed layer growth.

Improved mixing height monitoring

A. D. Griffiths et al.

Title Page

Abstract

Introduction

Conclusions

References

Tables

Figures

◀

▶

◀

▶

Back

Close

Full Screen / Esc

Printer-friendly Version

Interactive Discussion



If $C^{(i)} - (1 - \lambda\Delta t)C^{(i-1)} \geq 0$ then $D = 0$ and Eq. (A1) can be solved directly for $h_e^{(i)}$. Otherwise

$$D^{(i)} = \frac{C^{(i-1)} - (1 - \lambda\Delta t)C_r^{(i-1)}}{h_e^{(i-1)}} \frac{h_e^{(i)} - h_e^{(i-1)}}{\Delta t} \quad (\text{A2})$$

where C_r is the residual layer radon concentration entrained into the well-mixed box. It is possible for the mixing layer to grow through a discontinuity in C_p during a time-step. Taking this into account,

$$C_r^{(i-1)} = \frac{1}{h_e^{(i)} - h_e^{(i-1)}} \int_{h_e^{(i-1)}}^{h_e^{(i)}} C_p^{(i-1)}(z) dz. \quad (\text{A3})$$

Equations (A1), (A2) and (A3) are combined and solved implicitly for $h_e^{(i)}$ to advance h_e to the current time-step.

The radon profile, $C_p(z)$ is then advanced to the current time step, taking into account radioactive decay, so that

$$C_p^{(i)}(z) = \begin{cases} C^{(i)} & 0 \leq z < h_e^{(i)} \\ (1 - \lambda\Delta t)C_p^{(i-1)} & z \geq h_e^{(i)} \end{cases}. \quad (\text{A4})$$

Acknowledgements. We thank Jason and Diana Tremain for kindly permitting access to the Baldry research station, as well as Peter Graham and Adrian Element for their valuable assistance in the field.

Improved mixing height monitoring

A. D. Griffiths et al.

Title Page

Abstract

Introduction

Conclusions

References

Tables

Figures

◀

▶

◀

▶

Back

Close

Full Screen / Esc

Printer-friendly Version

Interactive Discussion



References

- Allegrini, I., Febo, A., Pasini, A., and Schiarini, S.: Monitoring of the nocturnal mixed layer by means of participate radon progeny measurement, *J. Geophys. Res.*, 99, 18765–18777, doi:10.1029/94JD00783, 1994. 6838
- 5 Arya, S. P.: Air pollution meteorology and dispersion, Oxford University Press, New York, USA, 1999. 6836
- Baars, H., Ansmann, A., Engelmann, R., and Althausen, D.: Continuous monitoring of the boundary-layer top with lidar, *Atmos. Chem. Phys.*, 8, 7281–7296, doi:10.5194/acp-8-7281-2008, 2008. 6837
- 10 Banta, R. M., Mahrt, L., Vickers, D., Sun, J., Balsley, B. B., Pichugina, Y. L., and Williams, E. J.: The very stable boundary layer on nights with weak low-level jets, *J. Atmos. Sci.*, 64, 3068–3090, doi:10.1175/JAS4002.1, 2007. 6850
- Barnes, J., Sharma, N., and Kaplan, T.: Atmospheric aerosol profiling with a bistatic imaging lidar system, *Appl. Opt.*, 46, 2922–2929, doi:10.1364/AO.46.002922, 2007. 6837
- 15 Chambers, S., Williams, A. G., Zahorowski, W., Griffiths, A., and Crawford, J.: Separating remote fetch and local mixing influences on vertical radon measurements in the lower atmosphere, *Tellus B*, 63, 843–859, doi:10.1111/j.1600-0889.2011.00565.x, 2011. 6838, 6843, 6846
- Conen, F. and Robertson, L. B.: Latitudinal distribution of radon-222 flux from continents, *Tellus B*, 54, 127–133, doi:10.1034/j.1600-0889.2002.00365.x, 2002. 6844
- 20 Conen, F., Neftel, A., Schmid, M., and Lehmann, B. E.: $N_2O/^{222}Rn$ – soil flux calibration in the stable nocturnal surface layer, *Geophys. Res. Lett.*, 29, 1025, doi:10.1029/2001GL013429, 2002. 6848
- Di Giuseppe, F., Riccio, A., Caporaso, L., Bonafé, G., Gobbi, G. P., and Angelini, F.: Automatic detection of atmospheric boundary layer height using ceilometer backscatter data assisted by a boundary layer model, *Q. J. Roy. Meteor. Soc.*, 138, 649–663, doi:10.1002/qj.964, 2012. 6837
- 25 Emeis, S., Münkel, C., Vogt, S., Müller, W. J., and Schäfer, K.: Atmospheric boundary-layer structure from simultaneous SODAR, RASS, and ceilometer measurements, *Atmos. Environ.*, 38, 273–286, doi:10.1016/j.atmosenv.2003.09.054, 2004. 6837
- 30

Improved mixing height monitoring

A. D. Griffiths et al.

Title Page

Abstract

Introduction

Conclusions

References

Tables

Figures

◀

▶

◀

▶

Back

Close

Full Screen / Esc

Printer-friendly Version

Interactive Discussion



Improved mixing height monitoring

A. D. Griffiths et al.

Title Page

Abstract

Introduction

Conclusions

References

Tables

Figures

◀

▶

◀

▶

Back

Close

Full Screen / Esc

Printer-friendly Version

Interactive Discussion



Emeis, S., Schäfer, K., and Münkel, C.: Surface-based remote sensing of the mixing-layer height – a review, *Meteor. Z.*, 17, 621–630, doi:10.1127/0941-2948/2008/0312, 2008. 6836, 6837

Emeis, S., Schäfer, K., and Münkel, C.: Observation of the structure of the urban boundary layer with different ceilometers and validation by RASS data, *Meteor. Z.*, 18, 149–154, doi:10.1127/0941-2948/2009/0365, 2009. 6837

Emeis, S., Schäfer, K., Münkel, C., Friedl, R., and Suppan, P.: Evaluation of the interpretation of ceilometer data with RASS and radiosonde data, *Bound.-Layer Meteor.*, 143, 25–35, doi:10.1007/s10546-011-9604-6, 2012. 6837

Fontan, J., Guedalia, D., Druilhet, A., and Lopez, A.: Une methode de mesure de la stabilite verticale de l'atmosphere pres du sol, *Bound.-Layer Meteor.*, 17, 3–14, doi:10.1007/BF00121933, 1979. 6838, 6842, 6843

Glickman, T. S.: Glossary of Meteorology, American Meteorological Society, 2 edn., available at: <http://amsglossary.allenpress.com/> (last access: 3 July 2012), 2000. 6850

Griffiths, A. D., Zahorowski, W., Element, A., and Werczynski, S.: A map of radon flux at the Australian land surface, *Atmos. Chem. Phys.*, 10, 8969–8982, doi:10.5194/acp-10-8969-2010, 2010. 6840, 6843, 6844, 6859

Grossi, C., Arnold, D., Adame, J., López-Coto, I., Bolívar, J., de la Morena, B., and Vargas, A.: Atmospheric ²²²Rn concentration and source term at El Arenosillo 100 m meteorological tower in Southwest Spain, *Radiat. Meas.*, 47, 149–162, doi:10.1016/j.radmeas.2011.11.006, 2012. 6838

Guedalia, D., Ntsila, A., Druilhet, A., and Fontan, J.: Monitoring of the atmospheric stability above an urban and suburban site using sodar and radon measurements, *J. Appl. Meteor.*, 19, 839–848, doi:10.1175/1520-0450(1980)019<0839:MOTASA>2.0.CO;2, 1980. 6838

Haefelin, M., Angelini, F., Morille, Y., Martucci, G., Frey, S., Gobbi, G. P., Lolli, S., O'Dowd, C. D., Sauvage, L., Xueref-Rémy, I., Wastine, B., and Feist, D. G.: Evaluation of mixing-height retrievals from automatic profiling lidars and ceilometers in view of future integrated networks in Europe, *Bound.-Layer Meteor.*, 143, 49–75, doi:10.1007/s10546-011-9643-z, 2012. 6837, 6841, 6847

Holford, D. J., Schery, S. D., Wilson, J. L., and Phillips, F. M.: Modeling radon transport in dry, cracked soil, *J. Geophys. Res.*, 98, 567–580, doi:10.1029/92JB01845, 1993. 6844

Keller, C. A., Huwald, H., Vollmer, M. K., Wenger, A., Hill, M., Parlange, M. B., and Reimann, S.: Fiber optic distributed temperature sensing for the determination of the nocturnal atmo-

Improved mixing height monitoring

A. D. Griffiths et al.

Title Page

Abstract

Introduction

Conclusions

References

Tables

Figures

◀

▶

◀

▶

Back

Close

Full Screen / Esc

Printer-friendly Version

Interactive Discussion



spheric boundary layer height, *Atmos. Meas. Tech.*, 4, 143–149, doi:10.5194/amt-4-143-2011, 2011. 6838

Lammert, A. and Bösenberg, J.: Determination of the convective boundary-layer height with laser remote sensing, *Bound.-Layer Meteor.*, 119, 159–170, doi:10.1007/s10546-005-9020-x, 2006. 6837

Mahrt, L.: Stratified atmospheric boundary layers, *Bound.-Layer Meteor.*, 90, 375–396, doi:10.1023/A:1001765727956, 1999. 6849, 6850

Mahrt, L.: Variability and maintenance of turbulence in the very stable boundary layer, *Bound.-Layer Meteor.*, 135, 1–18, doi:10.1007/s10546-009-9463-6, 2010. 6850

Martens, C. S., Shay, T. J., Mendlovitz, H. P., Matross, D. M., Saleska, S. R., Wofsy, S. C., Stephen Woodward, W., Menton, M. C., De Moura, J. M. S., Crill, P. M., De Moraes, O. L. L., and Lima, R. L.: Radon fluxes in tropical forest ecosystems of Brazilian Amazonia: night-time CO₂ net ecosystem exchange derived from radon and eddy covariance methods, *Global Change Biol.*, 10, 618–629, doi:10.1111/j.1365-2486.2004.00764.x, 2004. 6848

Moses, H., Stehney, A. F., and Lucas Jr., H. F.: The effect of meteorological variables upon the vertical and temporal distributions of atmospheric radon, *J. Geophys. Res.*, 65, 1223–1238, doi:10.1029/JZ065i004p01223, 1960. 6838, 6843

Münkel, C.: Mixing height determination with lidar ceilometers results from Helsinki Testbed, *Meteor. Z.*, 16, 451–459, doi:10.1127/0941-2948/2007/0221, 2007. 6837

Obrist, D., Conen, F., Vogt, R., Siegwolf, R., and Alewell, C.: Estimation of Hg⁰ exchange between ecosystems and the atmosphere using ²²²Rn and Hg⁰ concentration changes in the stable nocturnal boundary layer, *Atmos. Environ.*, 40, 856–866, doi:10.1016/j.atmosenv.2005.10.012, 2006. 6848

Pasini, A. and Ameli, F.: Radon short range forecasting through time series preprocessing and neural network modeling, *Geophys. Res. Lett.*, 30, 1386, doi:10.1029/2002GL016726, 2003. 6838

Schery, S. D., Gaeddert, D. H., and Wilkening, M. H.: Factors affecting exhalation of radon from a gravelly sandy loam, *J. Geophys. Res.*, 89, 7299–7310, doi:10.1029/JD089iD05p07299, 1984. 6844

Seibert, P., Beyrich, F., Gryning, S., Joffre, S., Rasmussen, A., and Tercier, P.: Review and intercomparison of operational methods for the determination of the mixing height, *Atmos. Environ.*, 34, 1001–1027, doi:10.1016/S1352-2310(99)00349-0, 2000. 6848

**Improved mixing
height monitoring**

A. D. Griffiths et al.

Title Page

Abstract

Introduction

Conclusions

References

Tables

Figures

◀

▶

◀

▶

Back

Close

Full Screen / Esc

Printer-friendly Version

Interactive Discussion



- Sesana, L., Caprioli, E., and Marcazzan, G. M.: Long period study of outdoor radon concentration in Milan and correlation between its temporal variations and dispersion properties of atmosphere, *J. Environ. Radioactiv.*, 65, 147–160, doi:10.1016/S0265-931X(02)00093-0, 2003. 6838, 6842
- 5 Sesana, L., Ottobriani, B., Polla, G., and Facchini, U.: ^{222}Rn as indicator of atmospheric turbulence: measurements at Lake Maggiore and on the pre-Alps, *J. Environ. Radioactiv.*, 86, 271–288, doi:10.1016/j.jenvrad.2005.09.005, 2006. 6838
- Sharma, N. C. P., Barnes, J. E., Kaplan, T. B., and Clarke, A. D.: Coastal aerosol profiling with a camera lidar and nephelometer, *J. Atmos. Oceanic Technol.*, 28, 418–425, doi:10.1175/2010JTECHA1482.1, 2011. 6837
- 10 Soler, M., Infante, C., Buenestado, P., and Mahrt, L.: Observations of nocturnal drainage flow in a shallow gully, *Bound.-Layer Meteor.*, 105, 253–273, doi:10.1023/A:1019910622806, 2002. 6846
- Stull, R. B.: *An Introduction to Boundary Layer Meteorology*, Springer, Dordrecht, The Netherlands, 1988. 6836
- 15 Sun, J., Lenschow, D., Burns, S., Banta, R., Newsom, R., Coulter, R., Frasier, S., Ince, T., Nappo, C., and Balsley, B.: Atmospheric disturbances that generate intermittent turbulence in nocturnal boundary layers, *Bound.-Layer Meteor.*, 110, 255–279, doi:10.1023/A:1026097926169, 2004. 6850
- 20 Szegvary, T., Conen, F., and Ciais, P.: European ^{222}Rn inventory for applied atmospheric studies, *Atmos. Environ.*, 43, 1536–1539, doi:10.1016/j.atmosenv.2008.11.025, 2009. 6844
- Trumbore, S. E., Keller, M., Wofsy, S. C., and Costa, J. M. D.: Measurements of soil and canopy exchange rates in the Amazon rain forest using ^{222}Rn , *J. Geophys. Res.*, 95, 16865–16873, doi:10.1029/JD095iD10p16865, 1990. 6848
- 25 Ussler, III, W., Chanton, J. P., Kelley, C. A., and Martens, C. S.: Radon 222 tracing of soil and forest canopy trace gas exchange in an open canopy boreal forest, *J. Geophys. Res.*, 99, 1953–1963, doi:10.1029/93JD02713, 1994. 6848
- Van de Wiel, B., Moene, A., Ronda, R., De Bruin, H., and Holtslag, A.: Intermittent turbulence and oscillations in the stable boundary layer over land. Part II: a system dynamics approach, *J. Atmos. Sci.*, 59, 2567–2581, doi:10.1175/1520-0469(2002)059<2567:ITAOIT>2.0.CO;2, 2002. 6850
- 30 Vickers, D. and Mahrt, L.: Evaluating formulations of stable boundary layer height, *J. Appl. Meteor.*, 43, 1736–1749, doi:10.1175/JAM2160.1, 2004. 6848

Vinuesa, J.-F. and Galmarini, S.: Characterization of the ^{222}Rn family turbulent transport in the convective atmospheric boundary layer, *Atmos. Chem. Phys.*, 7, 697–712, doi:10.5194/acp-7-697-2007, 2007. 6839

Vogelezang, D. and Holtslag, A.: Evaluation and model impacts of alternative boundary-layer height formulations, *Bound.-Layer Meteor.*, 81, 245–269, doi:10.1007/BF02430331, 1996. 6836

Weitkamp, C.: *Lidar: Range-Resolved Optical Remote Sensing of the Atmosphere*, Springer Series in Optical Sciences, Springer Science + Business Media, Boca Raton, USA, 2005. 6840

Whittlestone, S. and Zahorowski, W.: Baseline radon detectors for shipboard use: development and deployment in the First Aerosol Characterization Experiment (ACE 1), *J. Geophys. Res.*, 103, 16743–16751, doi:10.1029/98JD00687, 1998. 6840

Williams, A. G., Zahorowski, W., Chambers, S., Griffiths, A., Hacker, J. M., Element, A., and Werczynski, S.: The vertical distribution of radon in clear and cloudy daytime terrestrial boundary layers, *J. Atmos. Sci.*, 68, 155–174, doi:10.1175/2010JAS3576.1, 2011. 6838, 6839

Zhang, K., Feichter, J., Kazil, J., Wan, H., Zhuo, W., Griffiths, A. D., Sartorius, H., Zahorowski, W., Ramonet, M., Schmidt, M., Yver, C., Neubert, R. E. M., and Brunke, E.-G.: Radon activity in the lower troposphere and its impact on ionization rate: a global estimate using different radon emissions, *Atmos. Chem. Phys.*, 11, 7817–7838, doi:10.5194/acp-11-7817-2011, 2011. 6840, 6844

Improved mixing height monitoring

A. D. Griffiths et al.

Title Page

Abstract

Introduction

Conclusions

References

Tables

Figures

◀

▶

◀

▶

Back

Close

Full Screen / Esc

Printer-friendly Version

Interactive Discussion



Improved mixing height monitoring

A. D. Griffiths et al.

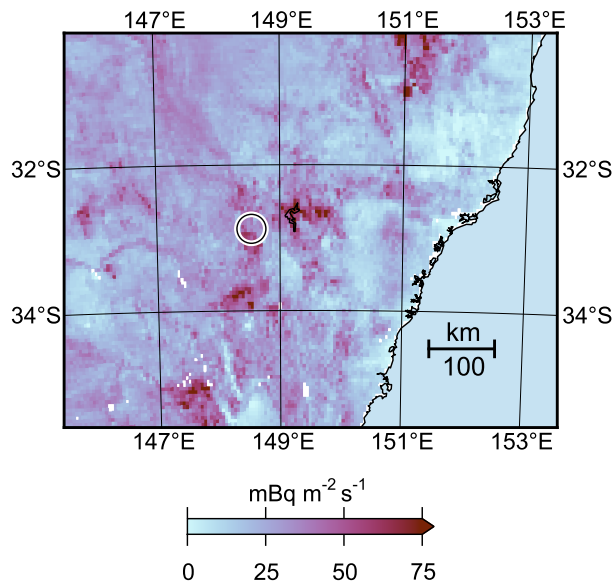


Fig. 1. The Baldry Hydrological Observatory (32.88° S, 148.54° E) and mean radon emissions (Griffiths et al., 2010).

Title Page

Abstract

Introduction

Conclusions

References

Tables

Figures

◀

▶

◀

▶

Back

Close

Full Screen / Esc

Printer-friendly Version

Interactive Discussion



Improved mixing height monitoring

A. D. Griffiths et al.

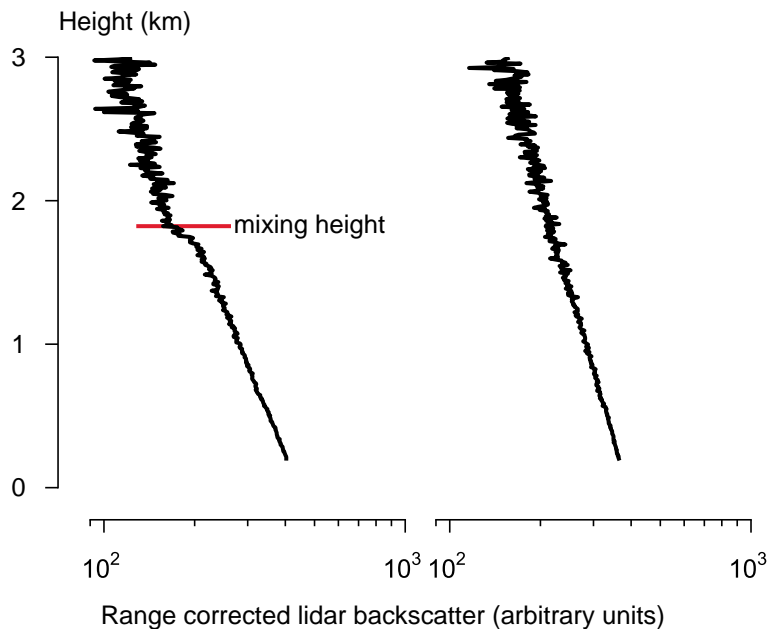


Fig. 2. Lidar profiles (mean of 18 000 laser shots) showing an example with a well defined mixing height (left), and one without a detectable aerosol layer (right).

[Title Page](#)[Abstract](#)[Introduction](#)[Conclusions](#)[References](#)[Tables](#)[Figures](#)[◀](#)[▶](#)[◀](#)[▶](#)[Back](#)[Close](#)[Full Screen / Esc](#)[Printer-friendly Version](#)[Interactive Discussion](#)

Improved mixing height monitoring

A. D. Griffiths et al.

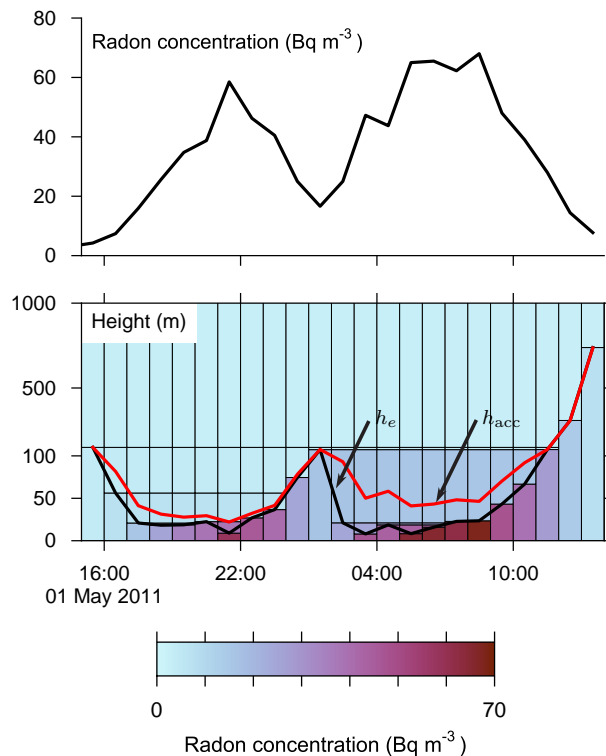


Fig. 3. Illustration of the procedure for deriving a mixing height from the diurnal composite radon time series. Local time (UTC + 10) is used in all figures.

Title Page

Abstract

Introduction

Conclusions

References

Tables

Figures

◀

▶

◀

▶

Back

Close

Full Screen / Esc

Printer-friendly Version

Interactive Discussion



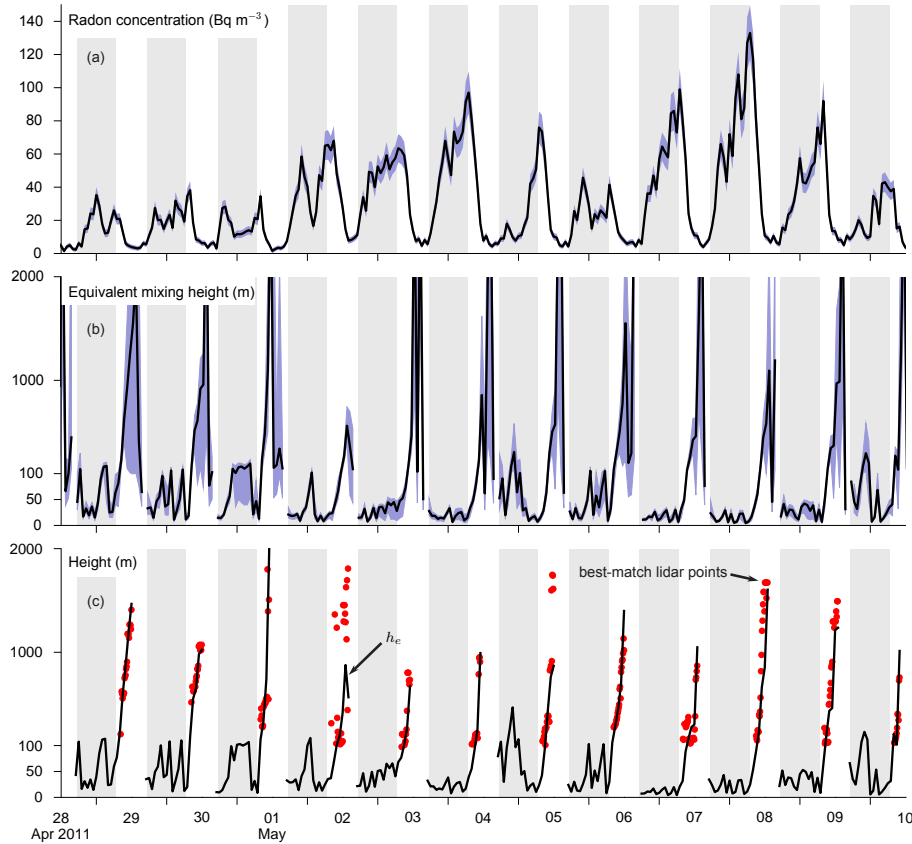


Fig. 4. Panel **(a)**: radon (shading indicates ± 1 standard deviation, approximately the 15th and 85th percentiles, of measurement uncertainty); **(b)** equivalent mixing height (shading extends to the 15th and 85th percentiles of an ensemble of models), and **(c)** lidar PBL height with calibrated h_e . Vertical shaded bars indicate night-time. The y-axes of **(b)** and **(c)** are magnified $5 \times$ below 100 m.

Improved mixing height monitoring

A. D. Griffiths et al.

Title Page

Abstract Introduction

Conclusions References

Tables Figures

◀ ▶

◀ ▶

Back Close

Full Screen / Esc

Printer-friendly Version

Interactive Discussion



Improved mixing height monitoring

A. D. Griffiths et al.

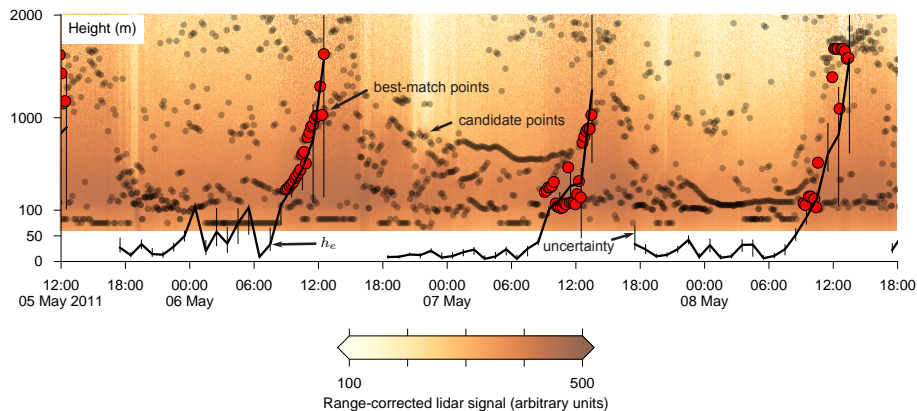


Fig. 5. A detailed view of lidar-derived and radon-derived mixing estimates over three days. The uncertainty in h_e is plotted at the the 15th and 85th percentiles.

[Title Page](#)[Abstract](#)[Introduction](#)[Conclusions](#)[References](#)[Tables](#)[Figures](#)[◀](#)[▶](#)[◀](#)[▶](#)[Back](#)[Close](#)[Full Screen / Esc](#)[Printer-friendly Version](#)[Interactive Discussion](#)

Improved mixing height monitoring

A. D. Griffiths et al.

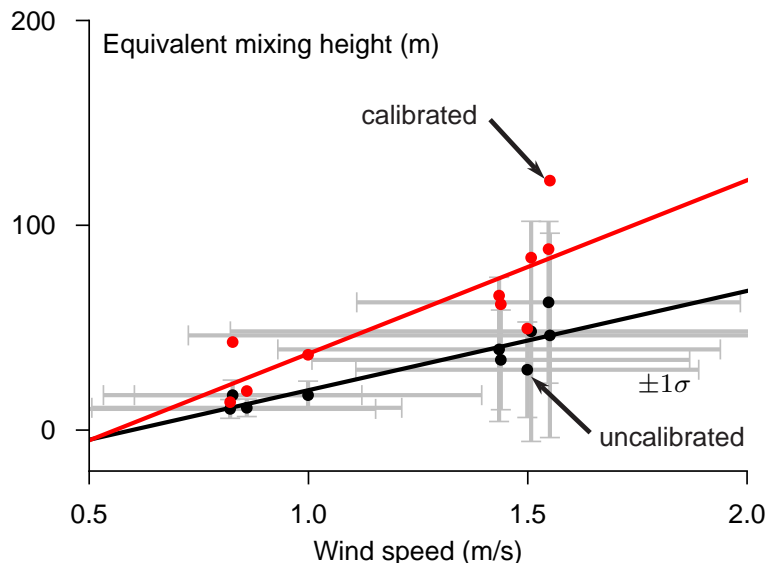


Fig. 6. Nightly average equivalent mixing height, h_e , versus average wind speed computed over the night time hours 1800–0600 lt. Bars show ± 1 standard deviation and linear least-squares trendlines have been fitted to the nightly means. Uncalibrated values are calculated from a constant assumed radon flux of $30 \text{ mBq m}^{-2} \text{ s}^{-1}$ (trendline: $y = 49x - 29$, $r^2 = 0.80$) and calibrated values are calculated from the nightly-varying flux obtained from merging the radon and lidar observations (trendline: $y = 84x - 47$, $r^2 = 0.69$).

[Title Page](#)[Abstract](#)[Introduction](#)[Conclusions](#)[References](#)[Tables](#)[Figures](#)[◀](#)[▶](#)[◀](#)[▶](#)[Back](#)[Close](#)[Full Screen / Esc](#)[Printer-friendly Version](#)[Interactive Discussion](#)

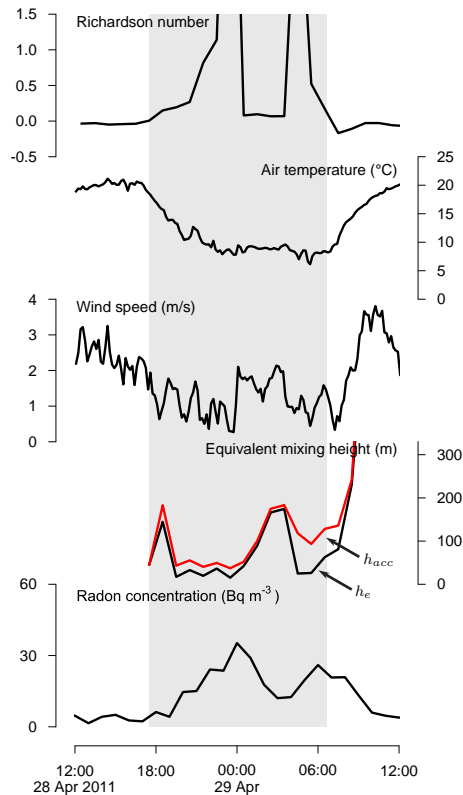


Fig. 7. Case study of a mixing event during a strongly stable night. The bulk Richardson number is computed from 2 m and 7.5 m wind speed and air temperature, air temperature and wind speed are shown at 2 m, the equivalent mixing height is shown as an hour-by-hour computation (h_e) as well as accumulation since nightfall (h_{acc}), and radon concentration is also measured at 2 m.

Improved mixing height monitoring

A. D. Griffiths et al.

Title Page

Abstract

Introduction

Conclusions

References

Tables

Figures

◀

▶

◀

▶

Back

Close

Full Screen / Esc

Printer-friendly Version

Interactive Discussion



Improved mixing height monitoring

A. D. Griffiths et al.

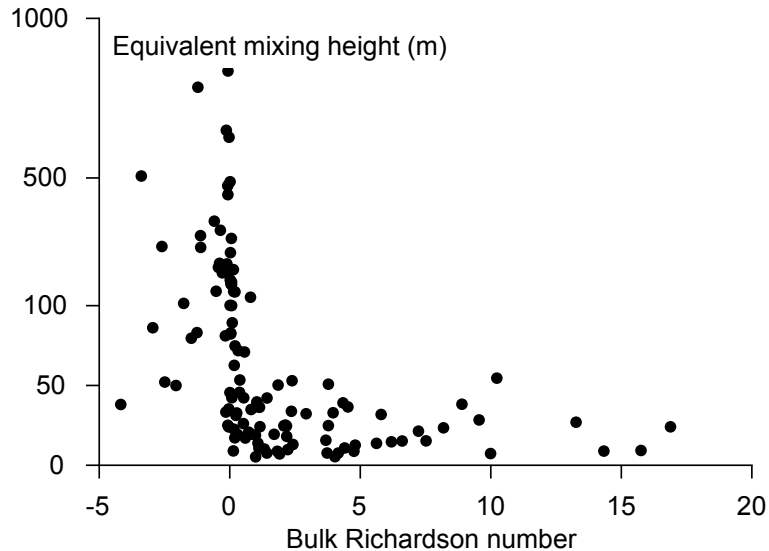


Fig. 8. Hourly measurements of calibrated equivalent mixing height, h_e , versus bulk Richardson number, Ri_b . The y-axis is magnified $5\times$ below 100 m and 163 data points are plotted.

[Title Page](#)[Abstract](#)[Introduction](#)[Conclusions](#)[References](#)[Tables](#)[Figures](#)[◀](#)[▶](#)[◀](#)[▶](#)[Back](#)[Close](#)[Full Screen / Esc](#)[Printer-friendly Version](#)[Interactive Discussion](#)